

# Matlab Based Simulation Toolbox for the Study and Design of Induction Motor FOC Speed Drives

A. COSTA,<sup>1</sup> M. VILARAGUT,<sup>1</sup> J. C. TRAVIESO-TORRES,<sup>2</sup> M. DUARTE-MERMOUD,<sup>2</sup> J. MUÑOZ,<sup>1</sup> I. YZNAGA<sup>1</sup>

<sup>1</sup>Centro de Investigaciones y Pruebas, Electroenergéticas, Facultad Eléctrica, Instituto Superior Politécnico "José Antonio, Echeverría", Ciudad de la Habana, Cuba

<sup>2</sup>Departamento de Ingeniería Eléctrica, Facultad de Ciencias Físicas y Matemáticas, Universidad de Chile, Santiago, Chile

Received 4 July 2007; accepted 19 October 2009

**ABSTRACT:** A new Matlab/Simulink based simulation toolbox for studying and designing induction motor field oriented control schemes is proposed in this article. It has advantages over other previous works published since it is modular, flexible, interactive, easy to use, and the results are closer to the experimental ones because it takes into account real complex effects, such as: motor core saturation, parameter variations with the speed and temperature, sensor signal digital processing, and inverter real voltage waveforms. These results has been successfully applied in teaching undergraduate and graduate courses at the authors' universities for building, identification and characterization of diverse control schemes, analysis of parameter effects, and design and test of new controllers for field oriented control schemes in induction motors. Beside the theoretical and computational basis of the toolbox, simulation results of an indirect field oriented control current regulated pulse width modulation scheme are presented in the article as example. ©2009 Wiley Periodicals, Inc. *Comput Appl Eng Educ*; Published online in Wiley InterScience (www.interscience.wiley.com); DOI 10.1002/cae.20396

**Keywords:** AC drives; induction motor; dynamic simulation; field oriented control; direct torque control

## INTRODUCTION

The increase of factory automation has been an important factor in worldwide industrial progress during the past several decades. Manufacturing lines in industrial plants typically involve one or more variable speed motor drives that serve to power conveyor belts, robot arms, paper mills, plastic and fiber processing lines, just to name a few [1].

Prior to 1950s all such applications required the use of DC motor drives. But, since the 1990s the use of AC drives started to be preferred [1]. In general AC drives often feature several advantages over their DC counterparts, such as: lower cost and maintenance, smaller motor size, and improved reliability [1–3].

However, the AC drives control scheme is more complex. There are three main schemes, the scalar V/f control, the field oriented control (FOC) and the direct torque control (DTC), each one with several variants. In these control schemes the use of an

inverter, controller blocks, and feedback signals processing is involved [1–4]. Besides, the induction motor (IM) itself is not as simple as the DC motor with separated field.

Perhaps, due to such complexity the study of AC drives is usually performed on dynamic simulations, which involve a lower cost than studies on a prototype but introduces some simplifications. We have the case of the software SIMULINK<sup>®</sup>, MATLAB<sup>®</sup> which has a power system toolbox for the study of electrical machines [5]. Several MATLAB based machine and AC drives simulations are also proposed in Ref. [6].

On the other hand, due to budget constraints, laboratories associated to certain courses in engineering curricula are being left out. They are often replaced by powerful and more realistic simulations. For instance, a virtual electric machine laboratory for simulating asynchronous machines, including magnetic saturation effects, is reported in [7,8] for teaching purposes.

A Matlab/Simulink realization of DC motor for speed control purposes is presented in Ref. [9]. They include different control methods such as field resistance, armature voltage, armature resistance and feedback control for DC motor drives.

Correspondence to: M. Duarte-Mermoud (mduartem@ing.uchile.cl).  
© 2009 Wiley Periodicals Inc.

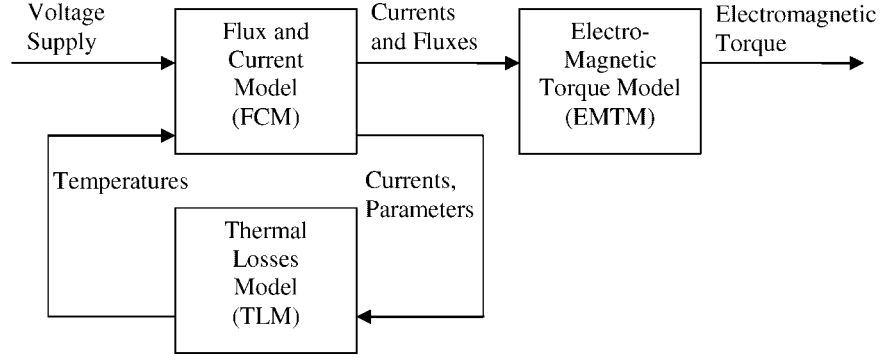


Figure 1 Block diagram of induction motor model.

In Ref. [10] an educational software is presented for neuro-fuzzy control of induction machines. The software has a flexible structure and graphical user interface allowing easy changes on neuro-fuzzy architecture and motor-load parameters.

A fully digital, real-time hardware-in-the-loop simulator on PC-cluster, of electric systems and drives for research and education purposes is presented in Ref. [11]. The simulator has two main subsystems; software and hardware. The software subsystem includes Matlab/Simulink environment, a C++ compiler and a real-time shell. The hardware subsystem includes a data acquisition card, the control board, the sensors, and the controlled motor.

In order to allow a deeper and more accurate study of AC drives and machines, the main nonlinearities present in this problem are considered in the simulation toolbox proposed in this article. Seven modules named Set Points, Controllers, Transformations, Inverters, Electro Mechanics, Sensors, and Miscellaneous were developed, each one containing several blocks. Beside, as example, six different FOC schemes ready to use were included. In the simulation real complex effects are considered, such as: motor core saturation, parameter variations with the speed and temperature, sensor signal digital processing, and inverter real voltage waveforms. Thus, compared to existing simulation methods, the results obtained from the toolbox are closer to the experimental ones, being also modular, flexible, interactive, and easier to use. These conclusions were obtained from teachers and students exposed to the proposed toolbox, employed in several courses on AC drives and for research purposes. Students and teachers were able to perform deeper study of machines and drives, with faster simulations as compared with previously used simulators, studying a larger number of cases in the same period of time. Besides, the characteristics of the toolbox developed here allowed students to make more complex homework at their own.

Basic concepts of AC drives considered in the simulation

toolbox are exposed in the second section of this article. In third section, the proposed Matlab/Simulink based simulation toolbox is described. Its blocks consider the effects of the core saturation and motor parameter variations with the speed and temperature, as well as the effects of the feedback signal processing and inverters actual voltage waveforms. An example of AC drives built-in based on the proposed toolbox is studied in fourth section, presenting the simulation results. Finally some conclusions are drawn in fifth section.

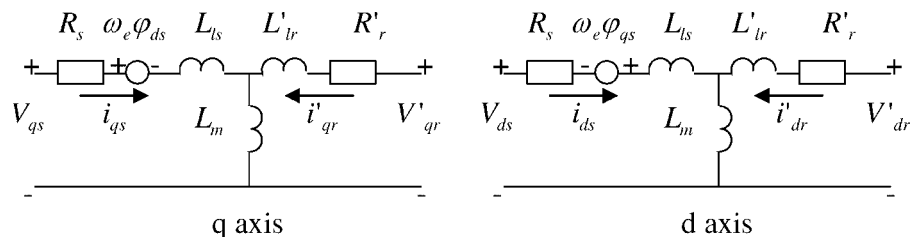
## BASIC CONCEPTS ON AC DRIVES

In this section we describe in a general form all the phenomena involved in the developed toolbox. We explain, from theoretical viewpoint, all the modules included in the toolbox for induction motor studies. Based on these equations toolbox modules were developed as explained in the third section.

### Induction Motor Model (Electro Mechanics)

In this study we employ the model of the induction motor based on references [1–6,12,13], including internal and external perturbations. The model consists of three modules: flux and current model (FCM), thermal losses model (TLM), and electromagnetic torque model (EMTM), as shown Figure 1. These modules are described in what follows.

The FCM solves the induction motor voltage equations, taking into account a stator reference frame. The  $d$ - $q$  equivalent circuit is used [13], but considering time-varying parameters due to skin effect in rotor impedance [14], influence of temperature on stator and rotor resistances and rotor leakage inductance variations due to the slip. The equations describing the FCM for stator and rotor are the following:



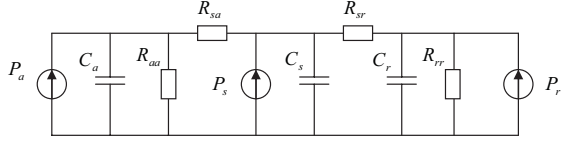


Figure 2 Induction motor thermal model.

$$\begin{aligned} V_{qs} &= R_s i_{qs} + \frac{d\phi_{qs}}{dt} + \omega_e \phi_{ds} \\ V_{ds} &= R_s i_{ds} + \frac{d\phi_{ds}}{dt} - \omega_e \phi_{qs} \\ V_{qr} &= R_r i_{qr} + \frac{d\phi_{qr}}{dt} + \omega_e \phi_{dr} \\ V_{dr} &= R_r i_{dr} + \frac{d\phi_{dr}}{dt} + \omega_e \phi_{qr} \end{aligned} \quad (2.1)$$

$$\begin{aligned} \phi_{qs} &= L_s i_{qs} + L_m i_{qr} \\ \phi_{ds} &= L_s i_{ds} + L_m i_{dr} \\ \phi_{qr} &= L_r i_{qr} + L_m i_{qs} \\ \phi_{dr} &= L_r i_{dr} + L_m i_{ds} \\ L_s &= L_{ls} + L_m \\ L_r &= L_{lr} + L_m \end{aligned} \quad (2.2)$$

where  $R$ ,  $L$ ,  $\omega_e$ ,  $V$ ,  $I$ , and  $\phi$  denote resistance, inductance, electrical frequency, voltage, current, and flux respectively, referred to rotor and stator on  $d$ - $q$  axes. As mentioned before parameters of these equations are time-varying taking into account the following aspects.

- Stator winding resistance  $R_s$  depends upon its temperature  $\theta_s$  according to the following equation

$$R_s = R_{s0}[1 + 0.004(\theta_s - \theta_0)] \quad (2.3)$$

where  $\theta_0$  is the environmental temperature.

- Rotor winding resistance  $R_r$  exhibits the same variation with temperature as stator winding but also is a function of the slip  $s$ , due to skin effect [14]. Its variation is given by the following the relations:

$$R_r = R_{r0}[1 + 0.004(\theta_r - \theta_0)], \quad R_{r0} = K_1 - K_2\sqrt{s} \quad (2.4)$$

- The rotor leakage inductance  $L_{lr}$  varies with slip, due to skin effect too [14], and can be calculated using the formula:

$$L_{lr} = K_3 - K_4\sqrt{s} \quad (2.5)$$

Parameters  $K_1$ ,  $K_2$ ,  $K_3$ , and  $K_4$  can be obtained from manufacturer's technical bulletin data or by means of no load tests [15,16].

- The magnetizing inductance  $L_m$  is considered as a function of the magnetizing  $I_m$  current with a per unit typical curve given by

$$L_{mpu} = K_{m3}I_m^3 + K_{m2}I_m^2 + K_{m1}I_m + K_{m0} \quad (2.6)$$

In this equation, the coefficients depend upon the type of motor [13].

Based on the knowledge of stator and rotor currents and the value of the corresponding parameters, the TLM determines the electrical losses in the motor stator, rotor and core. The electrical analog thermal model, with lumped parameters, for stator, rotor and core is shown in Figure 2. This module calculates the hot spot temperature of the stator winding, magnetic core and rotor winding, having as inputs the corresponding losses. Each node is assigned to a thermal capacitance  $C$  and the heat flowing through

thermal nodes is passed through thermal resistances  $R$  [15,17–19,24].

The corresponding thermal state space equations are:

$$\begin{aligned} \frac{d\theta_a}{dt} &= \frac{1}{C_a}[P_a - G_{oa}\theta_a + G_{as}\theta_s] \\ \frac{d\theta_s}{dt} &= \frac{1}{C_s}[P_s + G_{sa}\theta_a - G_{ss}\theta_s + G_{sr}\theta_r] \\ \frac{d\theta_r}{dt} &= \frac{1}{C_r}[P_r + G_{rs}\theta_s - G_{rr}\theta_r] \end{aligned} \quad (2.7)$$

where  $P_a$ ,  $P_s$ ,  $P_r$  are the magnetic core, stator winding, and rotor winding losses, respectively,  $G_{aa} = 1/R_{aa} + 1/R_{sa}$  is the total core thermal conductivity,  $G_{as} = G_{sa} = 1/R_{sa}$  is the mutual thermal conductivity between magnetic core and stator winding,  $G_{ss} = 1/R_{sa} + 1/R_{sr}$  is the total stator winding thermal conductivity,  $G_{sr} = G_{rs} = 1/R_{sr}$  is the mutual thermal conductivity between rotor winding and stator winding,  $G_{rr} = 1/R_{rr} + 1/R_{sr}$  is the total rotor winding thermal conductivity, and  $C_a$ ,  $C_s$ ,  $C_r$  are the corresponding magnetic core, rotor winding, and stator winding thermal capacitances.

The EMTM calculates the electromagnetic torque  $T_e$  based on the values of currents and flux linkages referred to the stator [1–6,12,13] utilizing the expression given by

$$T_e = 1.5p(\phi_{ds}i_{qs} - \phi_{qs}i_{ds}) \quad (2.8)$$

where  $p$  is the number of poles.

Finally, the well-known mechanical load model used in Refs. [1–6,12] considers the electromagnetic torque  $T_e$  and load torque  $T_m$  as inputs, and the rotor angular speed  $\omega_r$  as output. The equations are

$$\frac{d\omega_r}{dt} = \frac{1}{2H}(T_e - F\omega_r - T_m) \frac{d\theta}{dt} = \omega_r \quad (2.9)$$

where  $\theta$  is the rotor angular position.

## Inverters

All AC drives feed the machine through an inverter whose type depends on the speed drive scheme. There are two main inverter types, the voltage source inverter (VSI) and the current source inverter (CSI). The pulse width modulation (PWM) as VSI and the current regulated PWM (CRPWM) as CSI are widely used in FOC schemes with sinusoidal modulation. DTC instead is known by the use of a voltage selection table feeding a VSI [1–4].

The PWM is a VSI fed by the control voltages, usually with sinusoidal waveform and then sinusoidal modulation. Different current controllers can be designed as inner loop whose output feeds the inverter [2]. Figure 3 shows the block diagram of a PWM inverter used in a FOC scheme.

Conversely to VSI the CRPWM is a CSI and includes the current controller. It is fed by the output of the outer speed or flux controller loops. Here two main controllers are studied, the hysteretic (CRPWMH) and the sub-oscillatory one (CRPWMS) as it can be seen in Figures 4 and 5, respectively [2]. The hysteretic method guarantees a good dynamic behavior. It is simple, and it can be developed in an analog or digital way.

On the other hand, the sub-oscillatory or stationary controller is probably the most used method. The CRPWM with sub-oscillatory controller is shown in Figure 5.

The inverter used by DTC schemes has two main blocks, a look-up table and the inverter itself, as seen in Figure 6 and Table 1 [2].

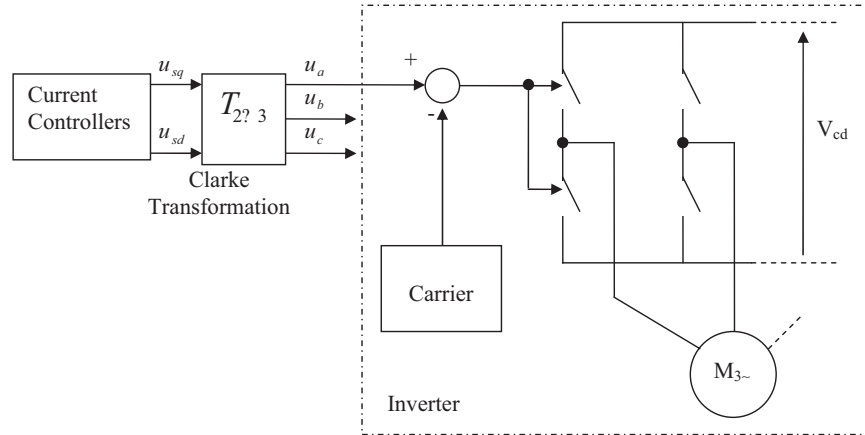


Figure 3 FOC with PWM inverter.

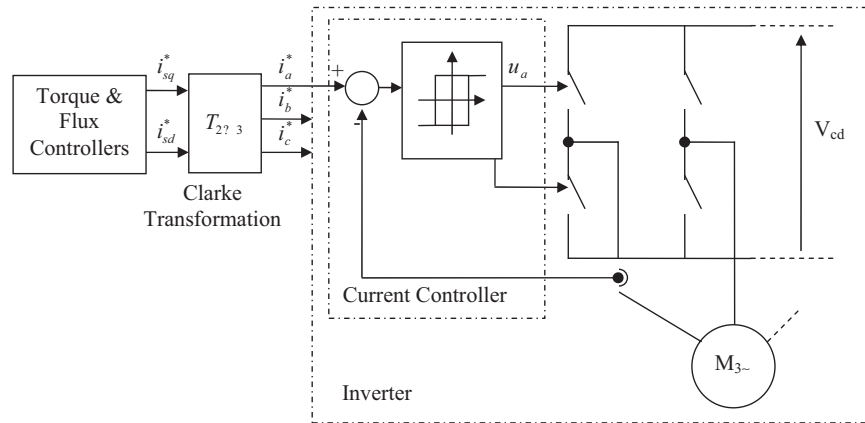
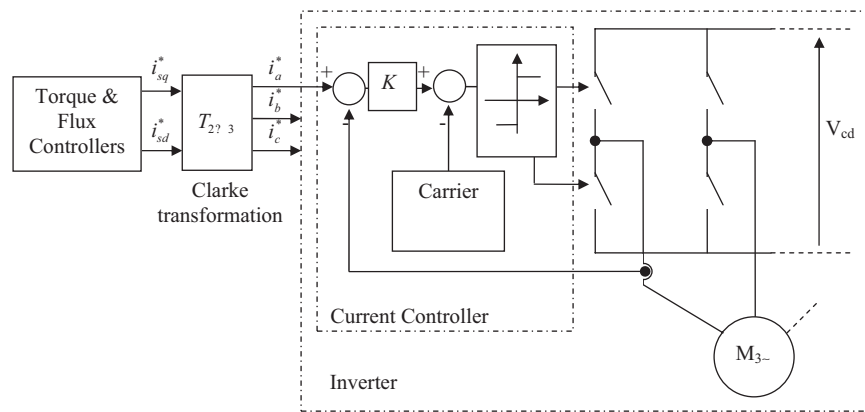


Figure 4 FOC with CRPWM and hysteric controller as inverter.



oller as inverter.

Figure 5 FOC with CRPWM and sub-oscillatory controller as inverter.

**Table 1** DTC—Classic Look-Up Table

$\Phi$	$\tau$	$S_1$	$S_2$	$S_3$	$S_4$	$S_5$	$S_6$
FI	TI	$V_2$	$V_3$	$V_4$	$V_5$	$V_6$	$V_1$
	T=	$V_0$	$V_7$	$V_0$	$V_7$	$V_0$	$V_7$
	TD	$V_6$	$V_1$	$V_2$	$V_3$	$V_4$	$V_5$
FD	TI	$V_3$	$V_4$	$V_5$	$V_6$	$V_1$	$V_2$
	T=	$V_7$	$V_0$	$V_7$	$V_0$	$V_7$	$V_0$
	TD	$V_5$	$V_6$	$V_1$	$V_2$	$V_3$	$V_4$

FI/FD, flux increase/decrease; TD/=I, torque decrease/equal/decrease;  $S_x$ : stator flux  $x$  sector;  $\Phi$ , stator flux controller output;  $\tau$ , torque controller output.

The stator flux sector is determined with the vector flux position  $\rho$ . Based on the sector and controller output of torque and flux, the look-up table determines the vector voltage output according to Figure 7.

**Coordinate Transformations**

In order to control a three-phase induction motor a two coordinate control scheme is usually used, as shown in Figures 8 and 9.

To convert sinusoidal signals from a two-phase control scheme output signals into a three-phase motor signals a transformation is needed, as well as the inverse operation [1–4,6]. To this extent Clarke Transformation is used and shown in Figure 8 where the  $a$  axis of the three-phase system is aligned with the axis  $d$  of the two-phase system.

To transform signals from two-phase system to three-phase system a  $T_{2 \rightarrow 3}$  transformation matrix is applied using the following relationship:

$$\begin{bmatrix} i_{sd} \\ i_{sq} \end{bmatrix} = \begin{bmatrix} 100 \\ 0\sqrt{3}/3 - \sqrt{3}/3 \end{bmatrix} \begin{bmatrix} i_{sa} \\ i_{sb} \\ i_{sc} \end{bmatrix}, \quad T_{3 \rightarrow 2} = \begin{bmatrix} 100 \\ 0\sqrt{3}/3 - \sqrt{3}/3 \end{bmatrix} \quad (2.10)$$

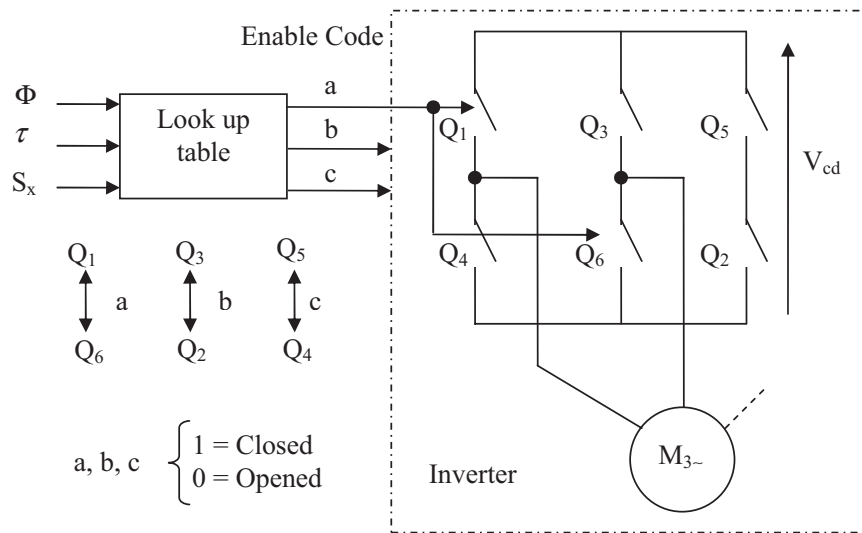


**Figure 6** DTC—Optimal table inverter.

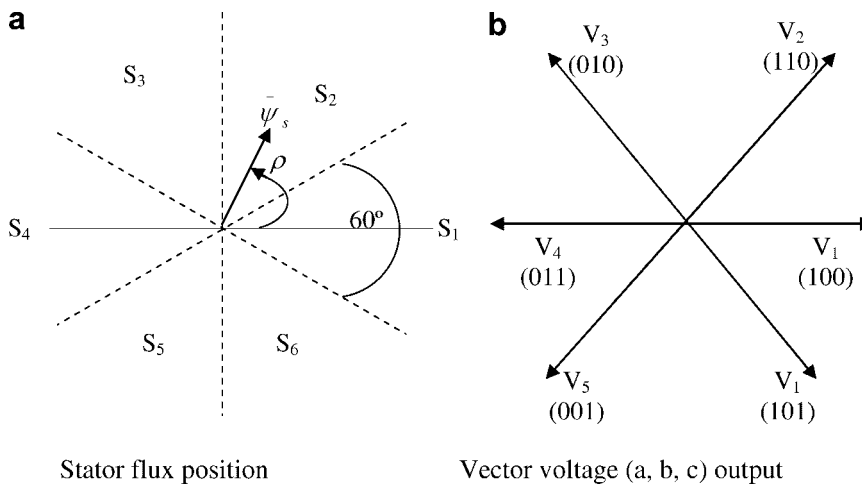


**Figure 7** Classic sectors input and vector voltage outputs.

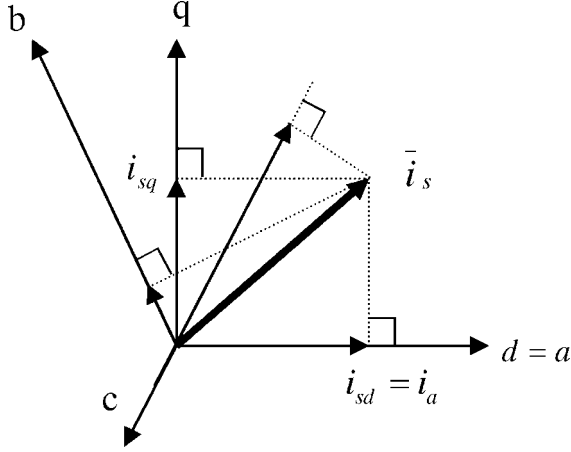


Figure 8 Clarke transformation applied to stator current.

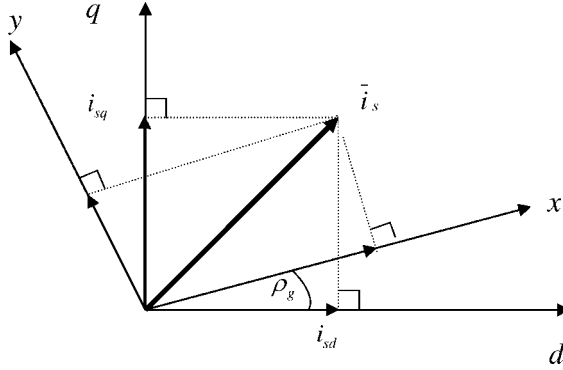


Figure 9 Park transformation applied to stator current.

To transform from three-phase signals system into a two phase one, the following transformation is applied

$$\begin{bmatrix} i_{sa} \\ i_{sb} \\ i_{sc} \end{bmatrix} = \begin{bmatrix} 10 \\ -1/2\sqrt{3}/2 \\ -1/2-\sqrt{3}/2 \end{bmatrix} \begin{bmatrix} i_{sd} \\ i_{sq} \end{bmatrix}, \quad T_{2 \rightarrow 3} = \begin{bmatrix} 10 \\ -1/2\sqrt{3}/2 \\ -1/2-\sqrt{3}/2 \end{bmatrix} \quad (2.11)$$

The Park transformation manages non-sinusoidal signals and it is used in control schemes (e.g., FOC) where amplitude and frequency of the sinusoidal wave are separately controlled. This transformation handles two-phase signals, but expressed in a different reference systems as shown in Figure 9 [1–4,6].

In Figure 9  $\rho_g$  is the position of the  $x$ – $y$  reference system with respect to the  $d$ – $q$  system.

The coordinate shift from a rotating system to a fixed system considers an  $e^{j\rho_g}$  transformation matrix and is given by

$$\begin{bmatrix} i_{sd} \\ i_{sq} \end{bmatrix} = e^{j\rho_g} \begin{bmatrix} i_{sx} \\ i_{sy} \end{bmatrix} = \begin{bmatrix} \cos \rho_g & -\text{sen } \rho_g \\ \text{sen } \rho_g & \cos \rho_g \end{bmatrix} \begin{bmatrix} i_{sx} \\ i_{sy} \end{bmatrix}, \quad (2.12)$$

$$e^{j\rho_g} = \begin{bmatrix} \cos \rho_g & -\text{sen } \rho_g \\ \text{sen } \rho_g & \cos \rho_g \end{bmatrix}$$

whereas the coordinate shift from a fixed system to a rotational system considers the inverse transformation  $e^{-j\rho_g}$ , which is the following

$$\begin{bmatrix} i_{sx} \\ i_{sy} \end{bmatrix} = e^{-j\rho_g} \begin{bmatrix} i_{sd} \\ i_{sq} \end{bmatrix} = \begin{bmatrix} \cos \rho_g & -\text{sen } \rho_g \\ \text{sen } \rho_g & \cos \rho_g \end{bmatrix}^{-1} \begin{bmatrix} i_{sd} \\ i_{sq} \end{bmatrix}, \quad (2.13)$$

$$\begin{bmatrix} i_{sx} \\ i_{sy} \end{bmatrix} = \begin{bmatrix} \cos \rho_g & \text{sen } \rho_g \\ -\text{sen } \rho_g & \cos \rho_g \end{bmatrix} \begin{bmatrix} i_{sd} \\ i_{sq} \end{bmatrix}$$

### Feedbacks Signal Processing

Sensor processing signal issues are also considered in the toolbox developed for simulation. Hall-effect current sensors, and their filters, and A/D converter quantization process, are taken into account. For the incremental encoder case, as speed sensor, filtering and quantization processes were considered.

There are several current control loop which are digital. Others, like the one used in the CRPWM inverter, are developed in an analog way. Digital loops involve the sampling and quantization processes. Due to the small sampling period used at present (from 40 to 300  $\mu$ s), it is possible to neglect the errors present when sampling frequency is small. However, since we work with digital numbers which can only take integer (discrete) values, the quantization process and its influence in the system dynamics needs to be considered. Besides, the AC drives use filters due to the inverter harmonics presence. Its presence affects the dynamic behavior of the system, which is considered here.

The current sensor could have three components, the sensor itself, a filter and an A/D converter. The A/D conversion considers the sampling, fixing and quantization processes. Usually, a Butterworth filter is also considered to improve the wave quality and to prevent aliasing effects considering a cutoff frequency. Its transfer function is

$$G(s) = \frac{K_{sc}}{(1/2\pi f_{oc})^2 s^2 + 1.41(1/2\pi f_{oc})s + 1} \quad (2.14)$$

where  $f_{oc}$  is the filter cutoff frequency and  $K_{sc}$  its gain.

The A/D converter considers a gain and a quantizer to achieve integer numbers. The converter gain is given by

$$K_{conv} = \frac{2^{nb-1}}{u_{cd}} \quad (2.15)$$

where  $nb$  is the bits number and  $u_{cd}$  is the converter maximum tension [20–22].

To measure rotor speed an *Incremental Encoder* with three pulse channels, is usually used. Two methods are considered by the speed driver in order to obtain the speed from the pulse signals; the *frequencymeter* and the *periodmeter*. The use of the *frequencymeter* method is considered for high speeds. The pulse number  $nps$  for the sampling period  $T_{sv}$  is determined by

$$nps = \frac{T_{sv}}{\alpha} \omega_r \quad (2.16)$$

where  $\alpha$  is the corresponding angle for each pulse, determined by  $\alpha = 2\pi/nenc$ , with  $nenc$  the number of pulse encoder per revolution. Finally we obtain

$$nps = \frac{T_{sv}nenc}{2\pi} \omega_r \quad (2.17)$$

Due to the dependences of the total angle and the angle  $\alpha$  of each pulse, this method introduces a quantification error which is higher for higher speeds. Thus, in this case a Butterworth filter (with cutoff frequency  $f_{0s}$ ) is also considered in order to improve the wave quality [20–22].

The use of the *periodmeter method* [20–22] is considered for low speeds. A high frequency clock is used to determine rotor speed through the expression

$$\omega_r = \frac{\alpha}{T_{enc}} \quad (2.18)$$

where  $T_{enc}$  is sampling period of the clock determined by  $T_{enc} = n_{hf}/f_{hf}$ , with  $n_{hf}$  being the clock pulse number of frequency  $f_{hf}$ . From these equations, the encoder speed output is determined as follows:

$$n_{hf} = \frac{2\pi f_{hf}}{n_{enc}} \omega_r \quad (2.19)$$

Finally, the speed of change from periodmeter to frequency-meter is denoted as  $w_c$ .

**MATLAB BASED SIMULATION TOOLBOX DESCRIPTION**

The different modules of the Matlab/Simulink based simulation toolbox developed in this study are shown in Figure 10a.

Each component of the proposed simulation toolbox designed and implemented in this article is explained in detail in what follows.

1. SET POINTS module: Allows choosing different test signals such as step, ramp, S type signals, etc., as can be seen in Figure 11a.

These blocks represents the main command signals used in closed-loop motor control studies, considering: single step, double step, saturated ramp, ramp and step, two way double ramp, single way double ramp, S starter and three-phase power supply. All the windows associated to these signals ask for the time of the different periods composing the command signals and amplitudes. As example, the window associated to double step box is shown in Figure 11b.

2. CONTROLLERS module: It considers a simple PID controller as well as a sub-oscillatory (see Fig. 5), hysteretic (see Fig. 4) and synchronic PID controllers, as shown in Figure 12a. These controllers can be used in any of the control loops of the FOC schemes shown in Figure 10b. For instance the hysteretic PID controller is used in the flux and torque control loops in the DTC scheme.

In all cases the controller parameters shall be defined as well as some practical values like the saturation voltage. In Figure 12b the window corresponding to the synchronic PID controller is shown as example.

3. TRANSFORMATIONS module: Considers the Clarke and Park transformations, as seen in Figure 13 and explained in coordinate Transformations Section.

These blocks do not require any parameter definition and they are based on relationships (2.10)–(2.13). All of them are

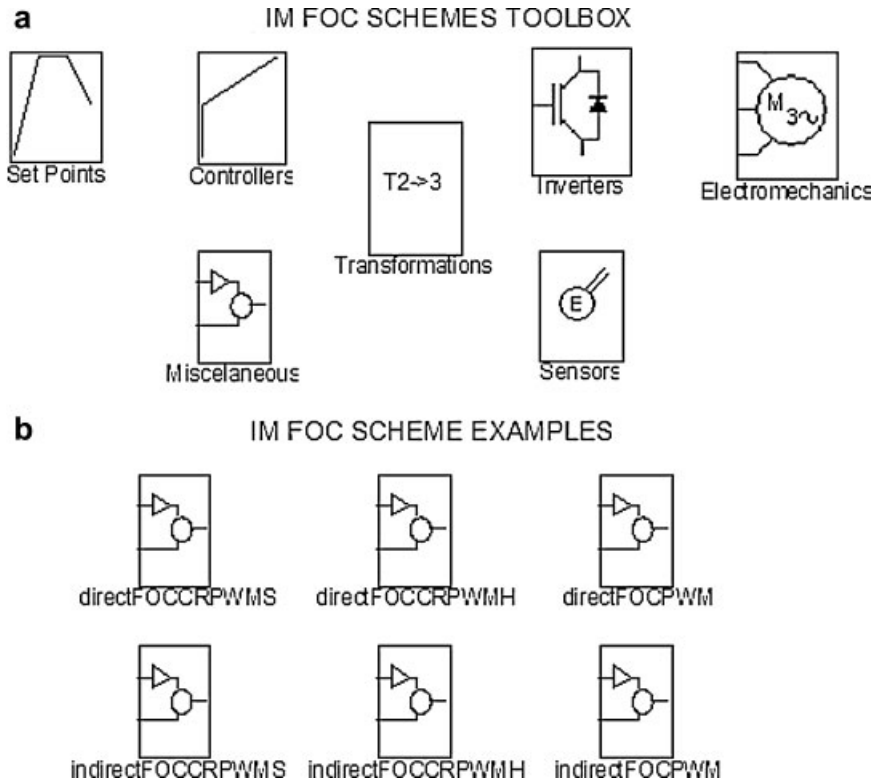


Figure 10 Matlab/Simulink based simulation toolbox main window.

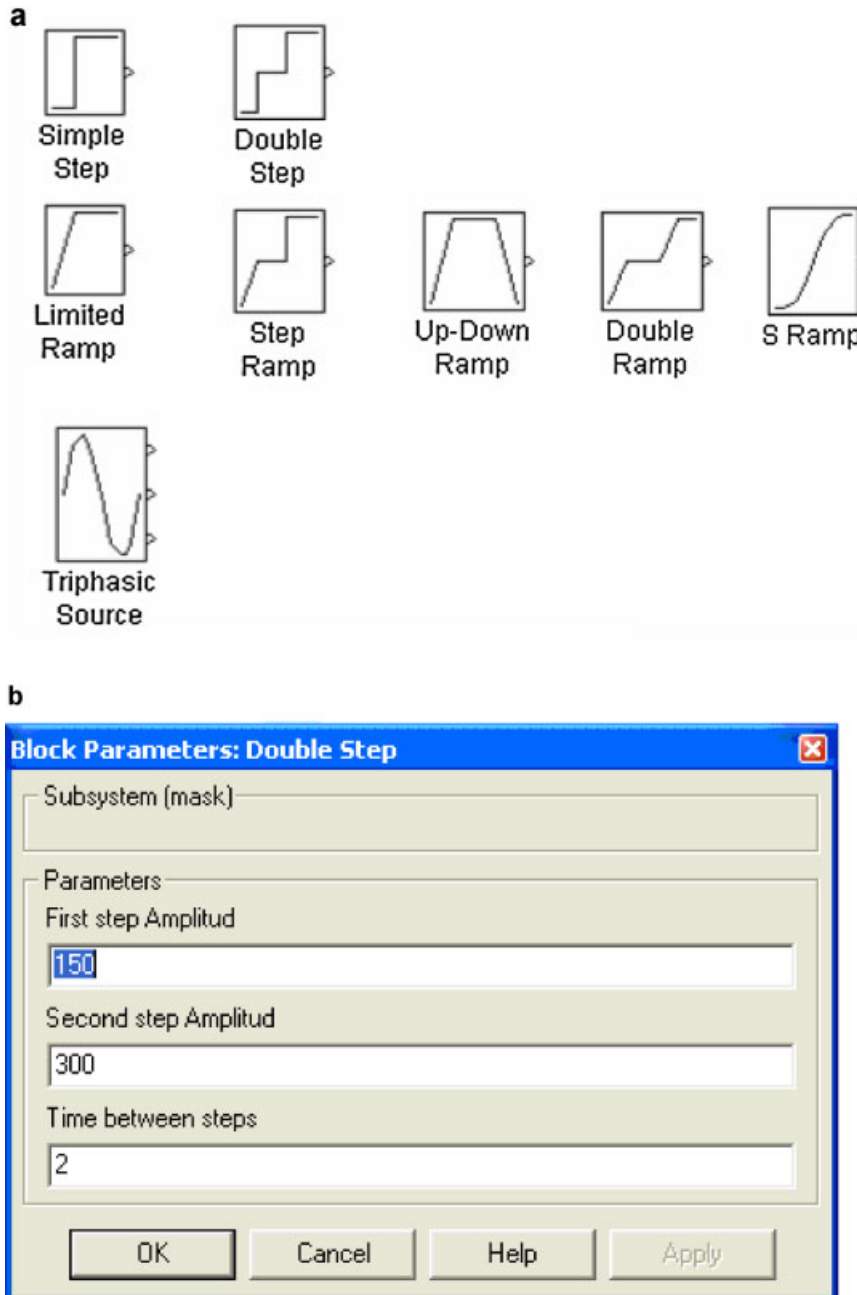


Figure 11 SET POINTS module. (a) General view. (b) Double step data input window.

fixed matrices, which in the case of the Park transformation depends on the  $\rho_g$  value ( $\rho_g$ ).

4. INVERTERS module: It is shown in Figure 14 and simulates the different types of PWM inverters as explained in Inverters Section.

These blocks consider the power electronic converters that usually feed the induction motor in vector control systems. Each window needs the definition of the commutation frequency, the regulator parameters and the DC voltage bus. In Figure 14b the window associated to PWM inverter is shown as illustrative example.

5. ELECTROMECHANICS module: It is exposed in Figure 15a.

The Simple Load module simulates the mechanical load on the motor axis. The Load with Perturbation module allows the possibility of including load disturbances at any instant of the simulation.

The input signals of the IM block are the three-phase voltages,  $u_a$ ,  $u_b$ ,  $u_c$ , the magnetizing current  $i_{mr}$  (in order to determine the magnetizing inductance), the rotor speed  $\omega_r$  and the stator revolving field speed  $\omega_g$ . The rotor speed comes from the mechanical load modules and the rest of the inputs from the

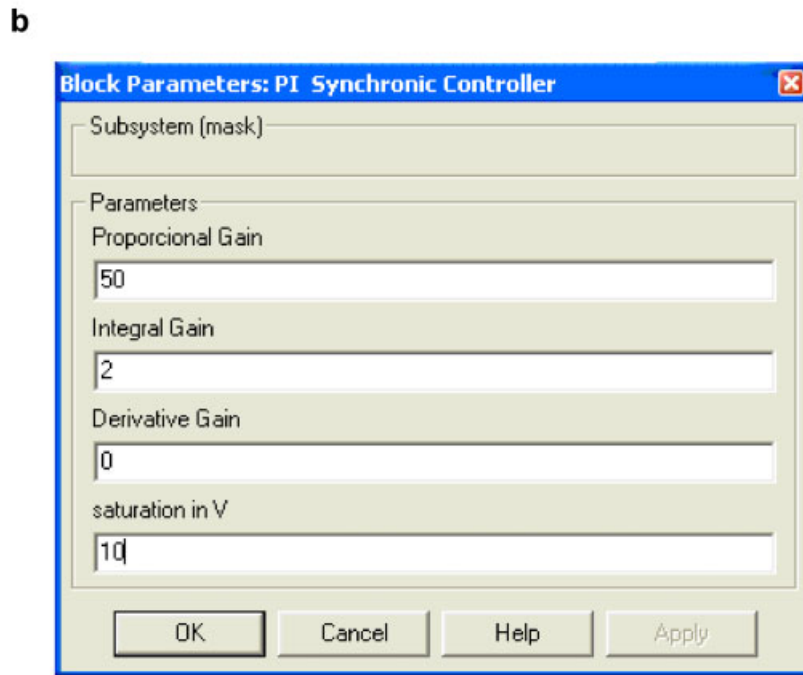
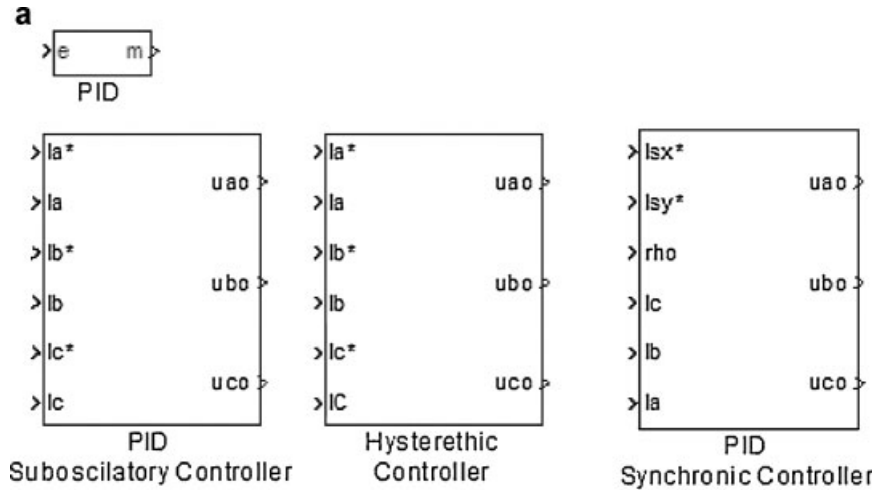


Figure 12 CONTROLLERS module. (a) General view. (b) PID synchronic controller data input window.

control system. The IM input window asks for the motor parameters and the mechanical load for the total inertia. The outputs are the three currents  $i_a$ ,  $i_b$ ,  $i_c$ , and the motor torque  $M_{em}$ , which is the input to the mechanical load module. A module considering the possibility of load disturbances is also included, asking for the load mechanical characteristic and the time for the application of the disturbance.

As additional information Figure 15b shows the window corresponding to IM module.

6. SENSORS module: It contains the simulation of the current acquisition system (including the filters), the encoder and the gearbox for simulating the mechanical transmission. There are three blocks involved as seen in Figure 16a; the encoder sensor block (for simulating the

inherent characteristic of this transducer such as the quantization error and its pulsed waveform), the current sensor block (that includes the filter and the A/D converter) and the gearbox position module (including the speed to position conversion).

The encoder window ask for the number of pulses per revolution, the cutoff frequency of the encoder filter, the periodmeter parameters, the sampling period and the processor clock frequency. The current data acquisition system needs the A/D converter analog voltage and number of bits and the filter frequency (see Feedbacks Signal Processing Section). The gearbox position block only asks for the gearbox ratio. Figure 16b illustrates the window associated to the encode sensor module as example.

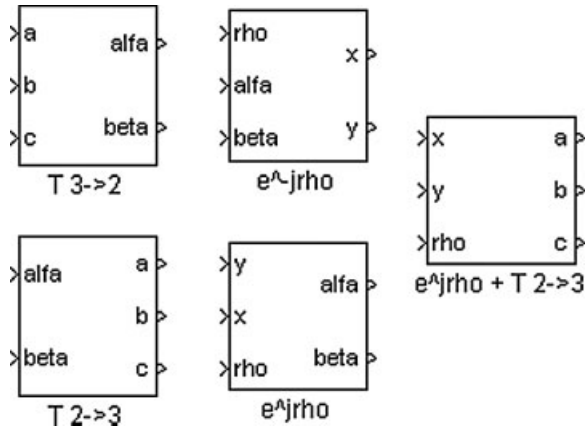


Figure 13 TRANSFORMATIONS module. Park and Clarke transformations.

7. MISCELANEOUS module: Simulates the flux level selector, and the slip and angle calculation for the indirect and direct field oriented control schemes respectively (see Fig. 17a).

The Direct FOC block calculates the rotor flux vector angle. Its inputs are the currents  $i_a$ ,  $i_b$ , and the rotor speed  $\omega_r$ . The outputs are the reference frame angle  $\rho_g$ , the estimated magnetizing current  $i_{mr}$ , the estimated electromagnetic torque  $M_{em}$ , and the frequency  $\omega_s$ . It asks for the estimated rotor time constant  $T_r$ ,

the torque constant and the number of poles of the motor. The Indirect FOC block calculates the slip  $\omega_s$  for the indirect field oriented vector based upon the two current components  $i_{sx}$ ,  $i_{sy}$  and the rotor speed  $\omega_r$ . It asks for the estimated rotor time constant and the number of poles of the motor. The Flux Selector block is used for choosing the constant torque operation zone or the constant power operation zone. It needs the nominal motor speed and the nominal excitation current. In Figure 17b the window corresponding to Flux Selector module is shown as example.

Based on the seven modules already explained different control schemes can be implemented for the IM. The toolbox developed include six different FOC schemes for IM (see Fig. 10b) that can be chosen by the user as ready to use examples or as a starting point to develop new control strategies, such as DTC. In the next section only one of these FOC scheme is simulated in detail to see how the toolbox works in general.

CASE STUDY

Simulation results of a speed drive control based on indirect FOC CRPWMS scheme are reported in this section. The following blocks were adjusted with the values of the parameters indicated in what follows.

- *Set Point:* A speed reference type Up-Down Ramp of amplitudes [0 180 180 0]rad/s and instants of time [0 25 35 50] s was used in the simulation.

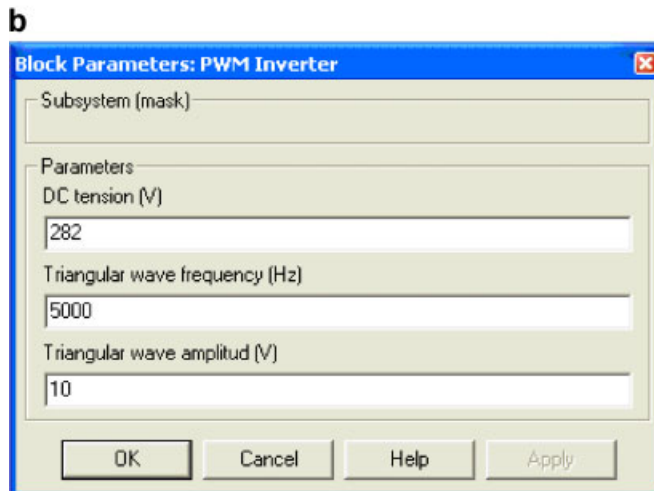
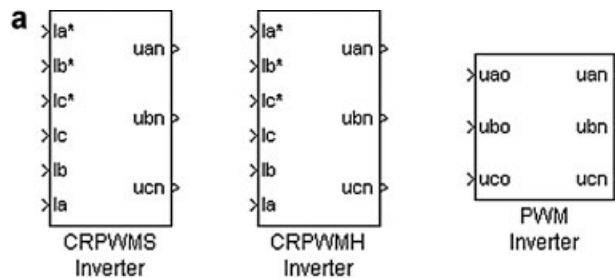


Figure 14 INVERTERS module. (a) General view. (b) PWM inverter data input window.

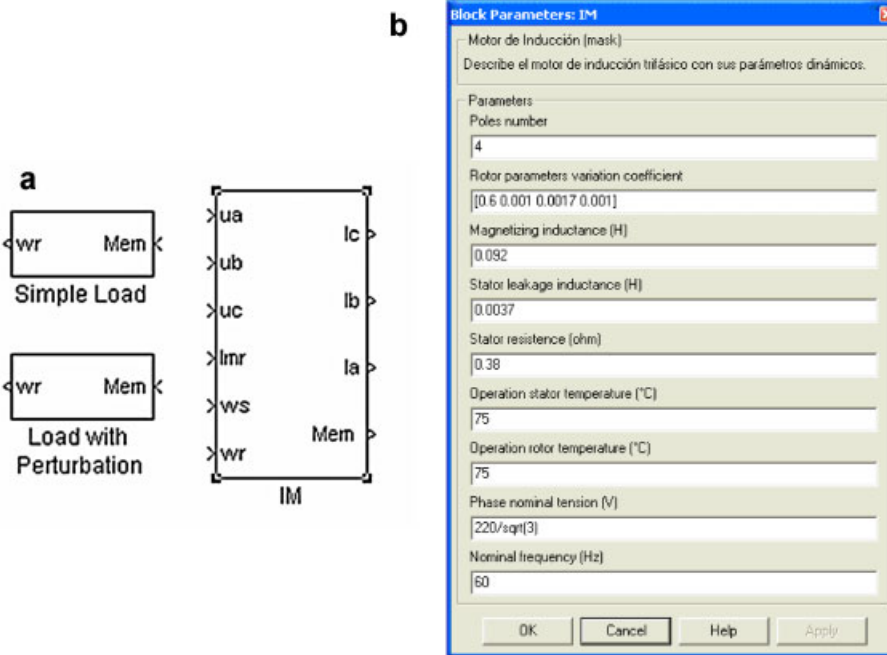


Figure 15 ELECTROMECHANICS module. (a) General view. (b) IM data input window.

- *Simple Load*: Electromechanic torque vector of [23 23 23] N m, speed vector of [0 80 200] rad/s, load inertia of 2.6 kg m<sup>2</sup>, motor inertia of 0.79 kg m<sup>2</sup>, and zero active torque load and initial rotor speed.
- *Induction Motor*: Four poles, rotor dependence parameters ( $K_1$ ,  $K_2$ ,  $K_3$ , and  $K_4$ ) of [0.0825 0.0144 0.000344 0.000135], magnetizing inductance of 0.0205 H, stator leakage inductance of 0.0006745 H, stator resistance of 0.0385  $\Omega$ , 75°C of running temperature for the stator and rotor, 220/ $\sqrt{3}$  nominal voltage, and 60 Hz.
- *CRPWMS*: proportional gain 50, integral gain 10, saturation voltage of 10 V, CD bus voltage of 295 V, 2 kHz frequency for the triangle wave with an amplitude of 10 V.
- *Indirect FOC*: with a rotor time constant  $T_r$  of 0.155 and four poles.
- *Flux Selector*: with 182.5 rad/s nominal angular rotor speed, and a nominal magnetizing current of 22 A.
- *Matlab Simulation Parameters*: 50 s stop time, 0.002 fixed step calculation method of ODE5 (Dormand-Prince) in automatic mode.

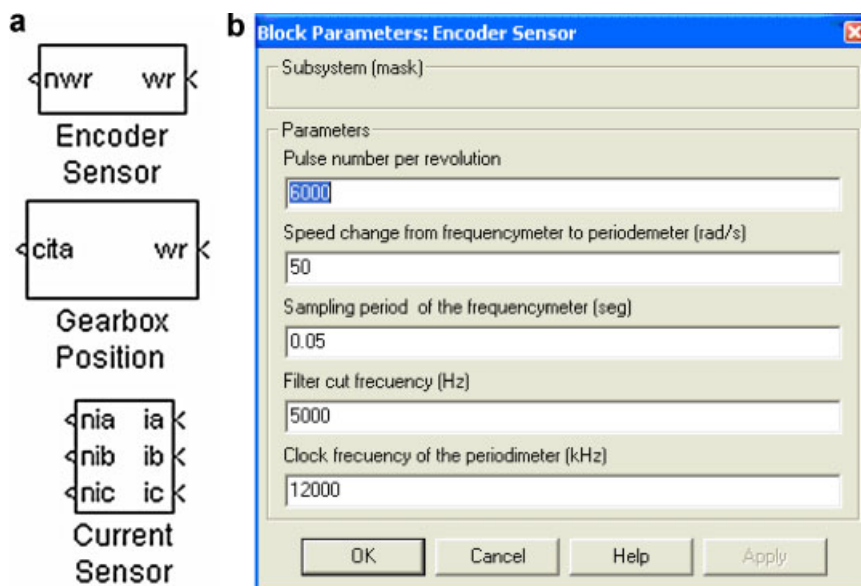


Figure 16 SENSORS module. (a) General view. (b) Encoder sensor data input window.

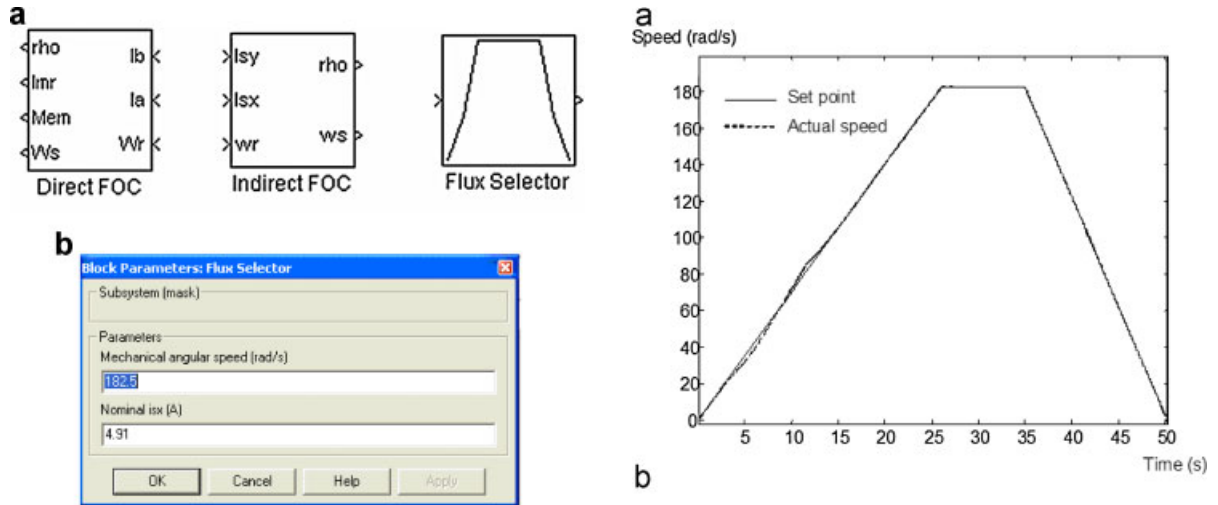


Figure 17 Miscellaneous module. (a) General view. (b) Flux selector data input window.

- *Thermal Parameters:* The following thermal parameters were used in the study:

$$G_{aa} = 400.21, 1/\Omega, G_{sa} = G_{as} = 2635.1, 1/\Omega,$$

$$G_{ss} = 0, 1/\Omega, G_{rs} = G_{sr} = 0.5167, 1/\Omega, G_{rr} = 88.74,$$

$$1/\Omega, G_{ra} = G_{ar} = 0, 1/\Omega, C_a = 640,000, \mu\text{F},$$

$$C_s = 16,883, \mu\text{F}, C_r = 85,685, \mu\text{F}$$

- *Sensor Parameters:* Other parameters used in the simulations for current and speed sensors are:

$$nenc = 5,000, \omega_c = 150 \text{ rad/s}, T_{sv} = 0.0005 \text{ s},$$

$$f_{0s} = 100 \text{ Hz}, f_{hf} = 1,000 \text{ kHz}, K_{sc} = 0.33,$$

$$f_{0c} = 1,000 \text{ Hz}, nb = 12, u_{cd} = 10 \text{ V}$$

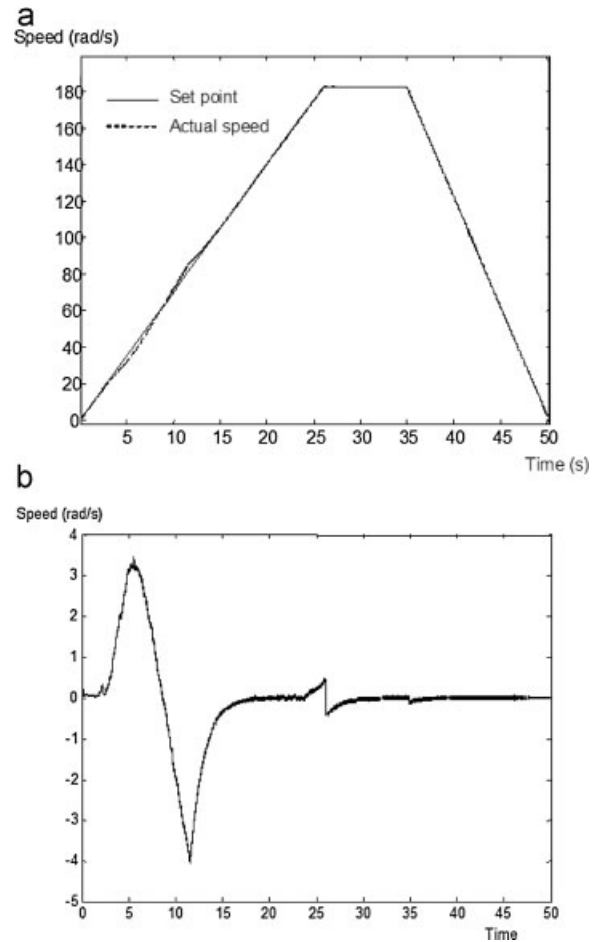


Figure 19 Results without considering sensors signal processing. (a) Set point and actual speed. (b) Speed error.

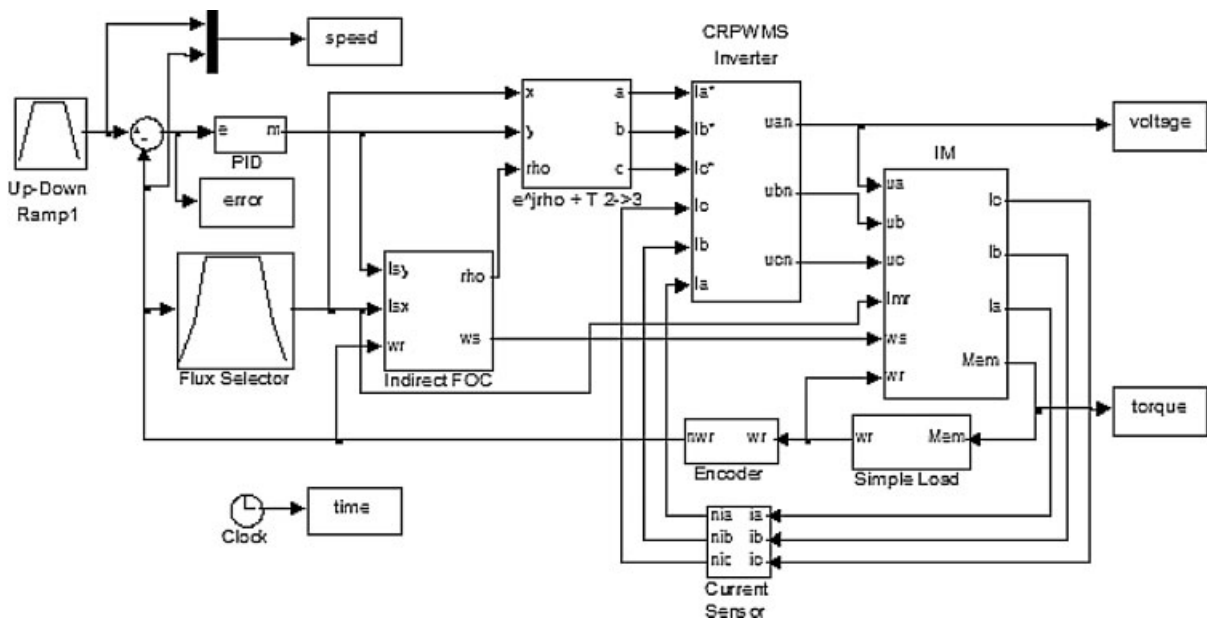
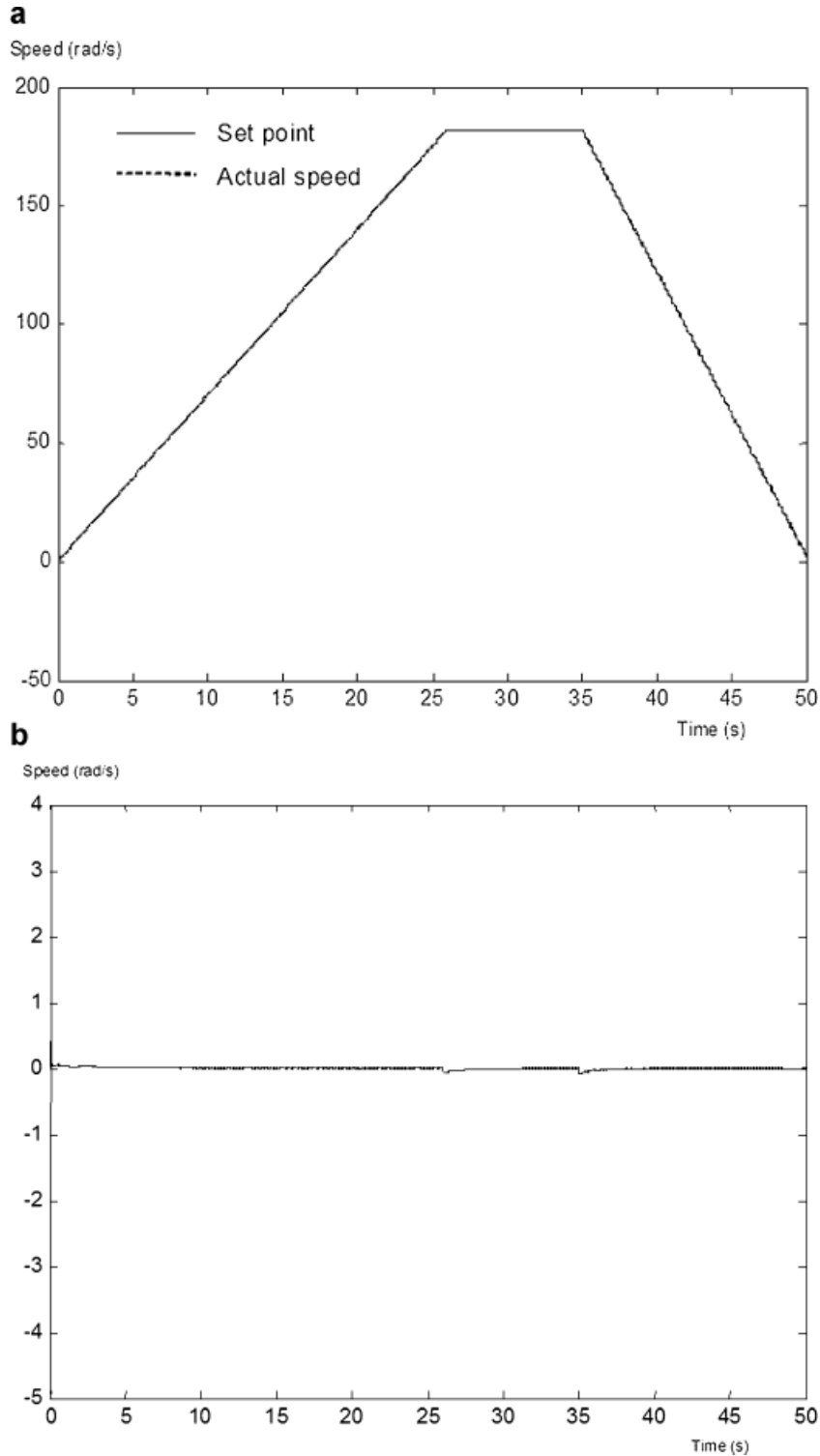


Figure 18 Block diagram for the case study.



**Figure 20** Results considering sensors processing. (a) Set point and actual speed. (b) Speed error.

In Figure 18 is shown the block diagram corresponding to the case studied in this article.

The speed and excitation controller were designed with the method explained in Ref. [23], the current limits and inverter

parameters utilized and the motion sensor and current data acquisition system were designed as in Refs. [20,22]. The simulation program was implemented with and without considering the effects of the speed sensor and the current data

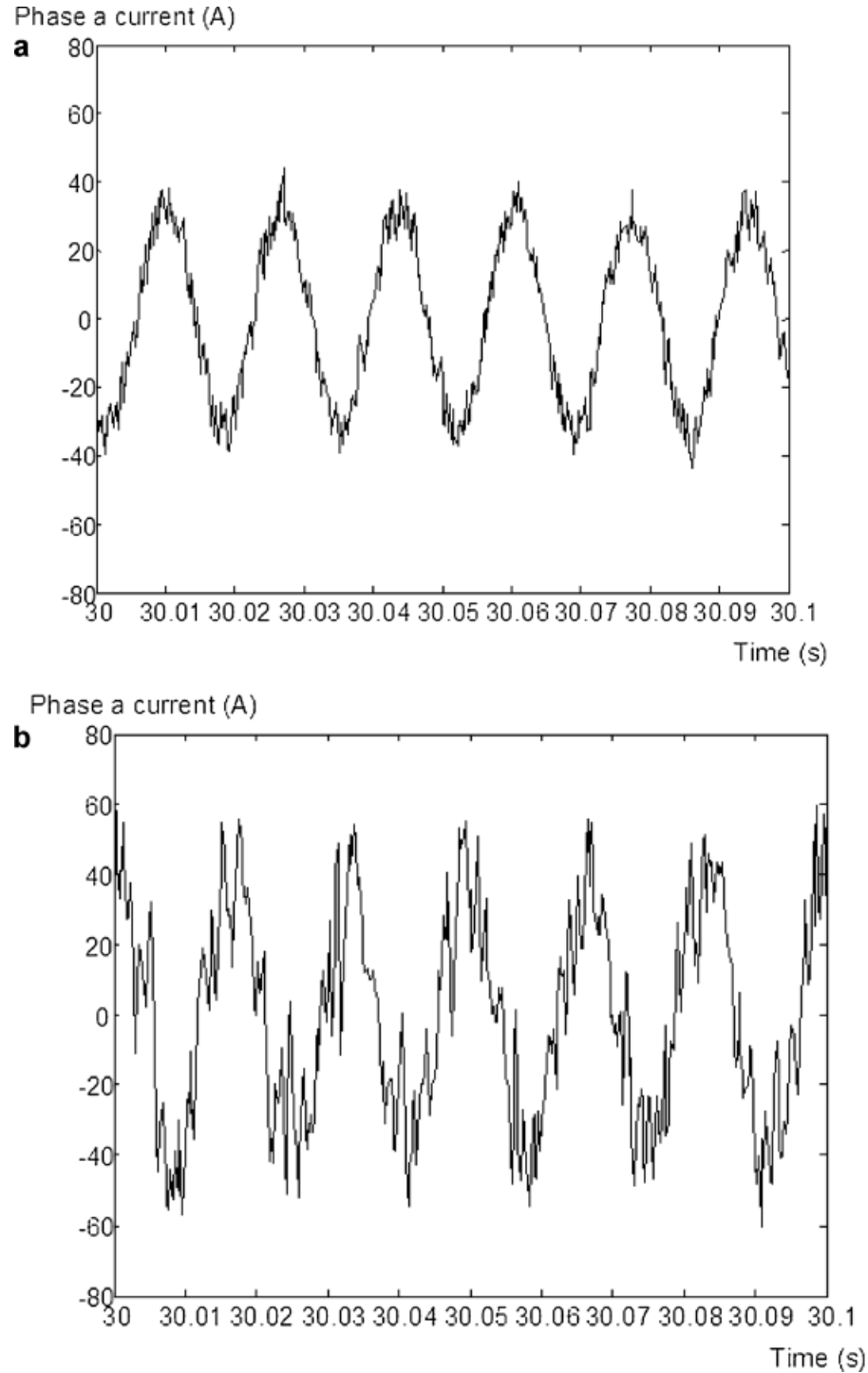


**Figure 21** Phase a current. (a) Without considering the sensors signal processing. (b) Considering the sensors signal processing.

acquisition system. In Figure 19a the comparison between the speed reference and the speed response without considering the sensors signal processing is depicted. In Figure 20a the same comparison is done but considering now the sensors signal processing. Figures 19b and 20b show the speed error in both cases.

Figures 21 and 22 show the evolution of current and voltage on phase *a*, with and without considering the sensor processing effects. A time interval from 30 to 30.1 s was chosen to show in detail the waveforms obtained from the simulations considering all the effects already described. From these figures it can be seen that current and voltage waveforms, with and without considering

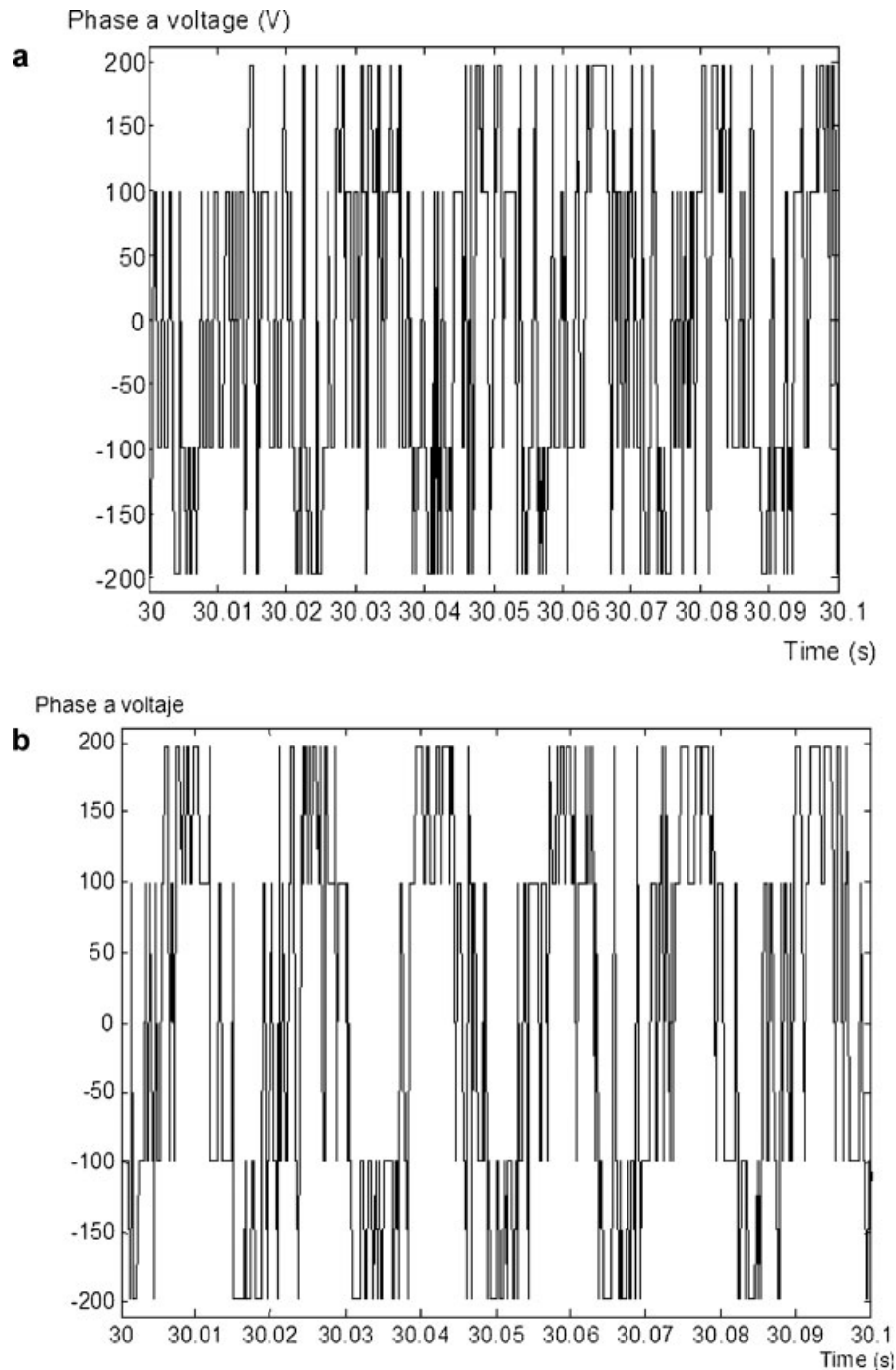


**Figure 22** Phase a voltage. a: Without considering the sensors signal processing. b: Considering the sensors signal processing.

the sensor dynamics, are quite close to real waveforms found in experimental setups.

Figures 21 and 22 are just a zoom of the true current/voltage waveforms to show in detail the waveform of those signals. The whole current/voltage signals were not shown for the sake of space. The interval 30 to 30.1 s was chosen as representative of the steady state regime. The influence of the sensor dynamics is clearly appreciated since Figure 21b exhibits more harmonic content and the instantaneous values are larger as compared with those in Figure 21a.

## PEDAGOGICAL AND TECHNICAL ADVANTAGES

### Pedagogical and Educational Issues

The software has been successfully used in several courses in Cuba (CIPEL-ISJAEP) and Venezuela. In Cuba, at undergraduate level, the software has been used in the course Automated Electrical Drives II given in the semesters 2006–2007, 2007–2008, and 2008–2009, covering 45 student on average per course. Thus, 135 students in total have been exposed

to the software to develop laboratory work associated to the course.

At graduate level (master degree program), the software was used in the course Control of Positioning Systems during the years 2007 and 2008, covering 36 students in all. The software was also used in the development of an E.E. Master Thesis in 2006.

In Venezuela, the software is being used at graduate level in laboratory courses as well as E.E. Theses, as part of the Master degree program given by CIPEL in three Venezuelan universities. Thirty students have been exposed to the software during 2007–2008 period.

Compared to existing simulation methods, the results obtained from the toolbox developed here are closer to the experimental ones, being also modular, flexible, interactive, and easier to use. These conclusions were obtained from teachers and students exposed to the proposed toolbox, employed in several courses on AC drives and for research purposes. Students and teachers were able to perform deeper studies of machines and drives, with faster simulations as compared with previously used simulators, studying a larger number of cases in the same period of time. Besides, the characteristics of the toolbox presented here allowed students to make more complex homework at their own.

### Technical Advantages

The current Matlab/Simulink software includes a toolbox for electrical drives containing limited models for electrical machines and control components since they are mainly linear and do not consider nonlinear phenomena whose influence in machine's behavior may become important. Some of these phenomena are indeed considered in the proposed toolbox.

One of the phenomena taken into account here is the rotor inductance and resistance variations due to skin effect. This effect exists and it is intentionally emphasized by manufacturers to increase the starting resistance (improving the starting torque) and to lower the resistance during the normal operation (achieving high efficiency). Something similar is obtained for the rotor inductance. The effects are not relevant in steady state regime studies but they make an important difference (produces large errors) while studying transient periods, for example, in control of electrical machines under FOC or other control schemes.

If rotor resistance is considered constant and equal to the nominal value the starting torque results much lower than the true one and it may happen that under high load torque the motor is not able to start in the simulation. On the contrary, if rotor resistance is considered constant and equal to the starting value the steady state regime speed will be lesser than the real one. The proposed software considers in a simple fashion this variation since the rotor resistance is made a function of the square root of slip.

Another improvement of the presented toolbox has to do with the encoder to measure the speed. This device is based on counting the number of pulses that can take only integer values. Different counting methods give raise to different quantization errors that may be important when determining the dynamical behavior of the control system. The quantization error and the sampling period are considered in the proposed toolbox.

Besides, the nonlinear nature of power converters, particularly the inverters, is also taken into account in the proposed software. This makes the simulation process faster.

Finally, as far as evidence of the toolbox advantages is concerned, we would like to mention that from Figure 19b an error different from zero in the transient response and during the stabilization is observed. This is due to field orientation loss. In fact, notice that the orientation block has a fixed rotor time constant  $T_r$  of 0.155, which is different from the true rotor time constant which varies due to speed and temperature variations of  $L_r$  and  $R_r$ , respectively. This error is not observed in Figure 20b when these variations are really considered.

### CONCLUSIONS

A new Matlab based simulation toolbox for the study and design of IM FOC schemes was presented in this article. The system is modular, flexible, interactive and easier to use. The obtained results are closer to the experimental ones since it considers the effects of core saturation and parameter variations of the induction motor due to the speed and temperature, as well as the effects of the sensor signal digital processing and inverters real voltage waveforms. As example, simulations results of a FOC CRPWM scheme using the developed toolbox were presented, from which the advantages of the proposed toolbox can be appreciated.

In the near future, additional controllers' blocks will be included considering: synchronous current control, fuzzy logic, neural network, sliding mode and adaptive passivity based controllers. The design of an OBSERVER module is also currently being developed.

### ACKNOWLEDGMENTS

The results reported in this article have been supported by CITMA-CONICYT through grant No. 2003-4-064.

### REFERENCES

- [1] B. K. Bose, Power electronics and variable frequency drives. IEEE Press Marketing, New York, 1997.
- [2] B. K. Bose, Modern power electronics and AC drives. Prentice Hall PTR, Upper Saddle River, NJ, 2002.
- [3] P. Vas, Sensorless vector and direct torque control. Oxford University Press, New York, 1998.
- [4] P. Vas, Electrical machines and drive. A space-vector theory approach. Oxford University Press, New York, 1992.
- [5] TransEnergie Technologies, under sublicense from Hydro-Quebec, and MathWorks, Inc., Copyright 1997-2002, "Asynchronous machine, Model the dynamics of a three-phase asynchronous machine, also known as an induction machine", Library Machines, from the SimPowerSystems. MATLAB, version 6.5.0.180913a release 13, June 18, 2002.
- [6] C. M. Ong, Dynamic simulation of electric machinery, using Matlab/Simulink. Prentice Hall PTR, New Jersey, 1998.
- [7] E. Tanyildizi and A. Orhan, A virtual electric machine laboratory for effect of saturation of the asynchronous machine application, Comput Appl Eng Educ 17 (2009), 422–428.
- [8] E. Tanyildizi and A. Orhan, A virtual electric machine laboratory for synchronous machine application, Comput Appl Eng Educ 17 (2009), 187–195.
- [9] S. Ayasun and G. Karbeyaz, DC motor speed control methods using MATLAB/Simulink and their integration into undergraduate

- electric machinery courses, *Comput Appl Eng Educ* 15 (2007), 347–354.
- [10] M. Gökbulut, C. Bal, and B. Dandil, A virtual electrical drive control laboratory: Neuro-fuzzy control of induction motors', *Comput Appl Eng Educ* 14 (2006), 211–221.
- [11] O. A. Mohammed and N. Y. Abed, Real-time simulation of electric machine drives with hardware-in-the-loop, *COMPEL: Int J Comput Math Electr Electron Eng* 27 (2008), 929–938.
- [12] P. Vas, Parameter estimation, condition monitoring, and diagnosis of electrical machines. Oxford University Press, New York, 1993.
- [13] P. Kovacs, Transient phenomena on electrical machines. Elsevier New York, 1984.
- [14] M. P. Kostenko and L. Piotrovsky, Electrical machines, I and II. Mir Publishers, Moscow, 1976, pp. 531–557.
- [15] E. Ruppert Filho and E. Avólio, Squirrel-cage induction-motor dynamics simulation using an electrical and thermal mathematical model based on manufacturer technical bulletins data and on technical standard statements, *Int J Power Energy Syst* 14 (1994), 13–16.
- [16] N. Galan, G. Ciumbulea, and S. Deleanu, Ratings and parameters of induction motors equivalent schemes, *Proc ICEM98 1* (1998), 239–242.
- [17] S. Zochol, E. Sweitzer, and A. Aliaga-Zegarra, Thermal protection of induction motors enhanced by interactive electrical and thermal models, *IEEE Trans Power Apparatus Syst* 103 (1984), 1749–1755.
- [18] A. H. Eltom and N. S. Moharari, Motor temperature estimation incorporating dynamic rotor impedance. IEEE PES Summer Meeting, Minneapolis, 1990, pp. 107–113.
- [19] P. H. Mellor, D. Roberts, and D. R. Turner, Lumped parameter thermal model for electrical machines of TEFC design. *IEE Proc B* 138 (1991), 205–218.
- [20] F. Briz del Blanco, Control vectorial del motor de inducción con identificación y adaptación a los parámetros de la carga. Ph.D. Thesis, Universidad de Oviedo, 1997.
- [21] M. V. Nuez-Amador, Simulación y control del motor de inducción por campo orientado. Ph.D. Thesis, CIPEL, Instituto Superior Politécnico José Antonio Echeverría ISPJAE, Ciudad de la Habana, 1998.
- [22] F. Briz, J. A. Cancelas, and A. Diez, Speed measurement using rotary encoders for high performance AC drives, *Proceedings of the 20th International Conference on Industrial Electronics, Control and Instrumentation, IECON 94*, 5–9 September 1994. Vol. 1, pp. 538–542.
- [23] W. Grantham and T. Vincent, *Modern control systems: Analysis and design*. John Wiley and Sons, U.K. 1993.
- [24] A. Costa and X. M. López-Fernández, Dynamic induction motor model considering skin effect and thermal performance. *Proceedings of the International Conference on Electrical Machines, ICEM 2002*, Bruges, Belgium.

## BIOGRAPHIES



**Angel Costa** has been an Electric Machines and Drives professor since 1966, investigating the development of industrial drives for Cuban industry. He has written many papers and books related to these themes and participated in many international and national conferences. He obtained the PhD degree from the Polytechnic Institute of Havana “Jose Antonio Echeverría” in 1987. He was a member of the Cuban Commission for the Development of Wind Energy. He has participated in many international projects and managed some of them. He is currently participating in the project for the introduction of Distributed Generation in the city of Luanda, Angola. His research interests are in the areas of Wind Energy, Electrical Drives and Distributed Generation development.



**Miriam Vilaragut** has been an Electric Machines and Drives professor since 1982, investigating in the introduction of Neural Networks in Electric Power Systems and Generators. She obtained the PhD degree from the Polytechnic Institute of Havana “Jose Antonio Echeverría” in 2002 with a special Cuban award for developing a system, based in Neural Network for the diagnosis of incipient faults in Synchronous Generator. She has written many papers for Cuban and international journals and publications. She is currently the Director of the Cuban “Centro de Investigaciones Electroenergéticas (CIPEL)”. Her research interests are in the areas of Electric Drives and Neural Network applications in Electrical Engineering.



**Juan C. Travieso-Torres** has 14 years of professional experience, including more than 9 years of teaching and research activities developed in parallel with his primary job. He is Doctor in Automatic Control, Master in Electrical Engineering, Electrical Engineer, and Bachelor in Electronics. He has been project manager in mining engineering projects with a budget between 50 and 130 millions dollars for BRASS Chile S.A; a corporate subject matter expert for Fluor, in the areas of DCS/PCS, control strategies, and variable speed drives; an Instrumentation and Control system Leader for Fluor and the Mining Company “Doña Inés de Collahuasi”; and an electrical/electronic maintainer.



**Manuel A. Duarte-Mermoud** received the degree of Civil Electrical Engineering from the University of Chile in 1977 and M.Sc., M.Phil., and Ph.D. degrees, all in electrical engineering, from Yale University in 1985, 1986 and 1988, respectively. From 1977 to 1979, he worked as Field Engineer at Santiago Subway. In 1979 he joined the Electrical Engineering Department of University of Chile, where he is currently Professor. His main research interests are in robust adaptive control (linear and nonlinear systems), system identification, signal processing and pattern recognition. He is focused on applications to mining and wine industry, sensory systems and electrical machines and drives. Dr. Duarte-Mermoud is a member of the IEEE and IFAC. He is past Treasurer and past President of ACCA, the Chilean National Member Organization of IFAC, and past Vice-President of the IEEE-Chile.



**Javier Muñoz** has been an Electric Drives and Automatic Control professor, since 2001 investigating in the development of Switched Reluctance Commutated Drives being applied in Cuban industry. He obtained the M.Sc. Degree from the Cuban “Centro de Investigaciones Electroenergéticas (CIPEL)” in 2005 and is working on his PhD dissertation on developing a sensorless SRC drive.



**Ivonne Yznaga** has been an Electric Drives professor since 2002, investigating in the simulation, analysis and development of different types of fault tolerant Electric Drives utilizing Artificial Intelligence. She obtained the Ph.D. degree from the Zhejiang University, Hangzhou, China in 2008. She is currently an Electrical Machines and Drives professor at the Cuban “Centro de Investigaciones Electroenergéticas (CIPEL)”. Her research interests are in the area of Artificial Intelligence applications in Electric Drives and Machines.